Mars Pathfinder Entry, Descent, and Landing Communications

G. E. Wood, S. W. Asmar, and T. A. Rebold
Communications Systems and Research Section

R. A. Lee
Network Engineering Section

Communication between the Mars Pathfinder spacecraft and the ground stations during the critical period of entry, descent, and landing required the development of a technique for and utilization of radio science open-loop instrumentation at the Deep Space Network. The signal carrier at X-band (8.43 GHz) was recorded with minimal gaps throughout this period when a complex sequence of events was being performed by the spacecraft. The carrier information was reconstructed and delivered to the Project in order to assess the engineering performance as well as possibly characterize the Martian upper atmosphere for future Mars missions. This article describes the technique, instrumentation, operations strategy, and signal processing task.

I. Introduction

On July 4, 1997, at 17:02 UTC, the Mars Pathfinder (MPF) spacecraft entered the atmosphere of Mars after a 7-month cruise period. The velocity of the spacecraft, with its progeny of a planetary lander and the Sojourner rover, was approximately 7 kilometers per second relative to the Martian atmosphere at the time of entry. In the ensuing 5 minutes, the spacecraft performed a complex sequence of events to safely decelerate and land at a predetermined destination in the Ares Vallis region of Mars' Northern Hemisphere. After landing, the sequence continued for nearly 4 hours as the lander employed an automated strategy to right itself, retract the air bags that cushioned its impact, and open its solar-cell-covered petals. It then waited silently for the Sun to rise and the Earth to reach a sufficient elevation angle to enable digital communications to stations of the Deep Space Network (DSN). The Pathfinder spacecraft, however, was not specifically designed to support communications with Earth during entry, descent, and landing (EDL). Nevertheless, it was possible to configure the spacecraft and DSN such that rudimentary communications could be maintained through a portion of that critical period.

The communications strategy purposely was kept simple; the objective was to record the X-band (8.43 GHz) carrier frequency along with semaphore signals that could corroborate key events of the lander's arrival and deployment on Mars. The recorded signals would enable flight path reconstruction, confirm sequence execution, and provide crucial data for analyses in case a mishap should occur. All communications during EDL were received solely by the Madrid Deep Space Communications Complex (MDSCC), with the 70-meter antenna, Deep Space Station 63 (DSS 63), being the prime aperture. Since the lander's signal would be dynamic in amplitude, frequency, and polarization, recordings were made

at both right- and left-hand circular polarizations (RCP and LCP) using open-loop receivers contained within the radio science DSCC signal processor (DSP) and the full-spectrum recorder (FSR). The receivers were aided with carefully constructed predicts that modeled the descent profile and ephemeris of Mars.

II. Overview of the EDL Sequence

Pathfinder's EDL events were controlled by autonomous software running in the spacecraft's attitude and information management (AIM) computer. This software was designed with the recognition that the spacecraft was a planetary lander and the requisite algorithms to support EDL were necessarily an inherent behavior of such a lander. Hence, the control of EDL events was by special capabilities built into the AIM software and not a true "sequence." However, colloquial usage has dubbed this software the "EDL sequence" and no distinction will be made from here on. During the events of EDL, the spacecraft continuously transmitted an X-band carrier. Superimposed on the carrier were semaphores confirming the execution of events at key times as the sequence progressed. The semaphores were implemented using two different schemes. Prior to landing, semaphores were constructed by switching between two selectable subcarrier frequencies in the spacecraft. Once on the surface, the semaphores were produced simply by turning on and off an unmodulated X-band carrier. Highlights of the EDL sequence are illustrated in Fig. 1, with the following paragraphs providing a narrative expanding on those events.

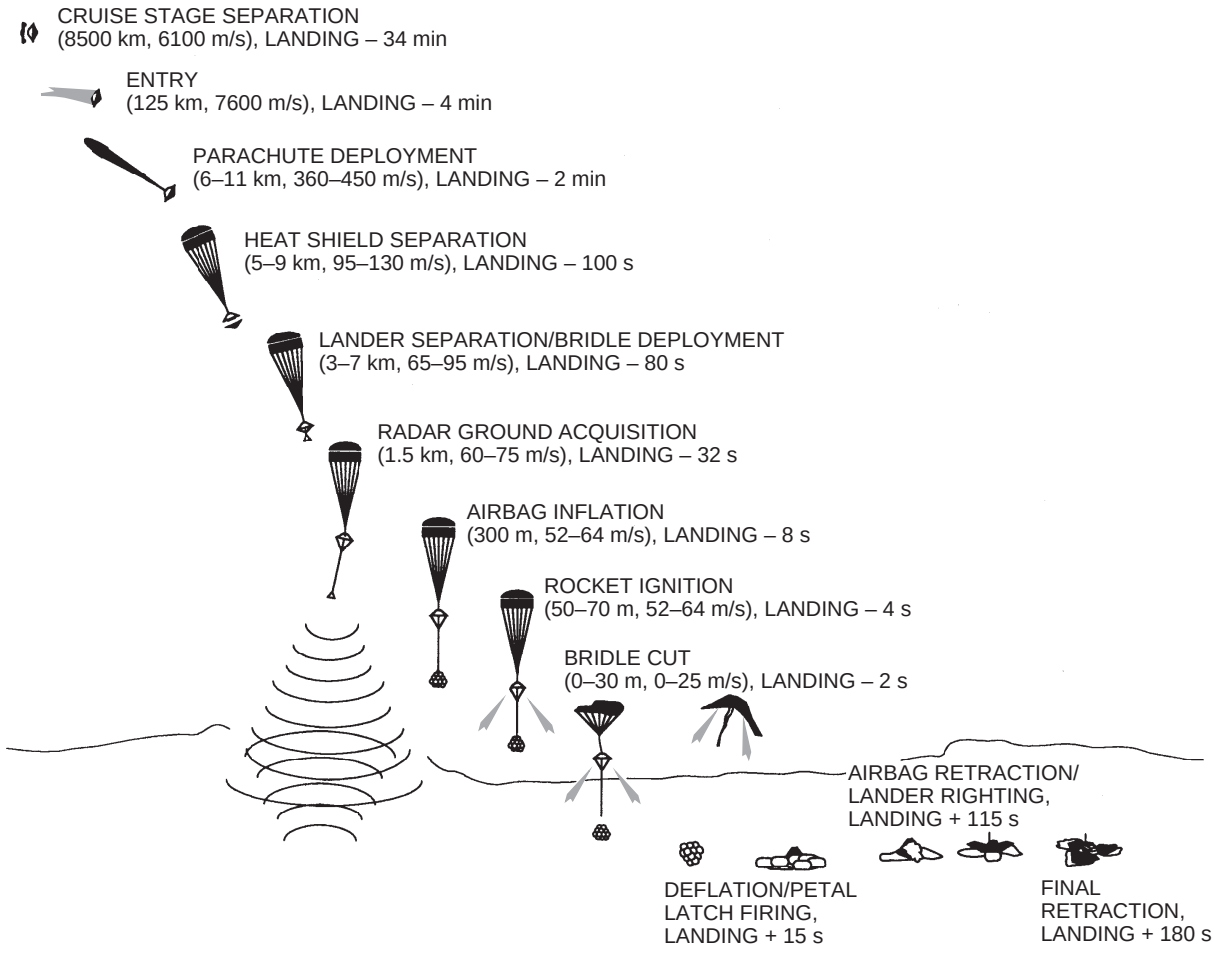

Fig. 1. Mars Pathfinder entry, descent, and landing sequence on July 4, 1997, with landing at 10:07 a.m. PDT (Earth received time).

The events of EDL began 90 minutes before atmospheric entry. At that time, the chlorofluorocarbon coolant of the spacecraft cruise stage was vented into space. The cruise stage had provided cooling, power, and attitude control for the 7 months since launch but was now being conditioned for jettison since it was not designed to withstand the rigors of atmospheric entry. Venting of the coolant meant that temperatures within the lander would begin to rise, a consideration that was factored into estimates of the crystal oscillator reference when making DSN tuning predicts. At 32 minutes before entry, the spacecraft switched to a 5-bits-per-second uncoded data rate, which narrowed the data spectrum around the telemetry subcarrier. Simultaneously, the X-band modulation index was set to 60 deg, which produced a carrier suppression of 6 dB. These actions configured the downlink to provide nearly equal power between each of the subcarrier first side bands and the carrier itself, thus enhancing the probability of detecting semaphores during the entry and descent phases.

Thirty minutes before entry, the cruise stage was jettisoned under control of the EDL sequence. Departing with the cruise stage was the medium-gain antenna (MGA), which had served for all communications during the 7 months since launch. The spacecraft would now use the backshell low-gain antenna (BLGA), which was mounted on the backshell that protected the rear hemisphere of the lander during entry. When the cruise stage separated, the signal at Earth disappeared for nearly 30 seconds. This was the result of the communications path being obstructed by the departing cruise stage. When the signal returned, it was about 7-dB weaker, as expected, since the broad beam of the BLGA resulted in reduced antenna gain. At 15 minutes before entry, the spacecraft sent a single calibration semaphore. The calibration semaphore provided a representative sample of switching from the low subcarrier (22.5 kHz) to the high subcarrier (360 kHz) while the downlink signal was still strong and stable.

At entry, the spacecraft was protected by its heat shield, which served to decelerate the craft until reaching an altitude of approximately 10 kilometers. Signals during this interval were extremely dynamic, and analyses of their character will be presented later in this article. Under control of the EDL sequence, a parachute was then deployed, which further slowed the spacecraft's descent. With the parachute out, the heat shield was released and a semaphore was issued to signal the event. The spacecraft then dropped below the backshell on a bridle that acted as a tether between the parachute and backshell and the lander itself. As the spacecraft descended out of the backshell, the BLGA was shed and communications continued using a lander-fixed low-gain antenna (LGA). When the bridle was fully extended, a second semaphore was issued to mark the event. Sixteen seconds later, the lander switched to a linearly polarized descent antenna (DEA) that provided improved downlink levels due to the ever increasing antenna aspect angle with Earth on the horizon of Mars.

A third semaphore was issued when the lander's radar altimeter sensed an altitude of 600 meters above the planet's surface. The airbags were then inflated; three solid rocket motors were ignited within the backshell high above the tethered lander; and the bridle was cut, allowing the lander to free-fall to the surface of Mars. The bounce from impact, coupled with the horizontal velocity at the time of bridle cut, resulted in the lander rolling for more than 1 minute before coming to a stop. Remarkably, when the lander stopped, it was oriented with its base down. The lander was right side up with the DEA being almost vertical and nearly 3 meters above the surface of Mars rather than stuffed in the soil or a Martian pothole! What greater serendipity could be hoped for—the signal was stable and clear.

From cruise stage separation until roll stop on the surface, the spacecraft utilized four different antennas. At the same time, the aspect angle to Earth varied over nearly 90 deg. These two effects together caused the downlink signal to vary over a range of more than 20 dB with the received signal-to-noise ratio (P_t/N_o) at times dropping well below 16 dB-Hz. That level was estimated as the threshold for real-time visibility. A priori calculation of the received signal level for the RCP component of the downlink is displayed in Fig. 2.

Frequency dynamics during entry were equally as dramatic as those of amplitude dynamics. During the 5 minutes of descent, the X-band sky frequency rose by more than 200 kHz. The slope and total

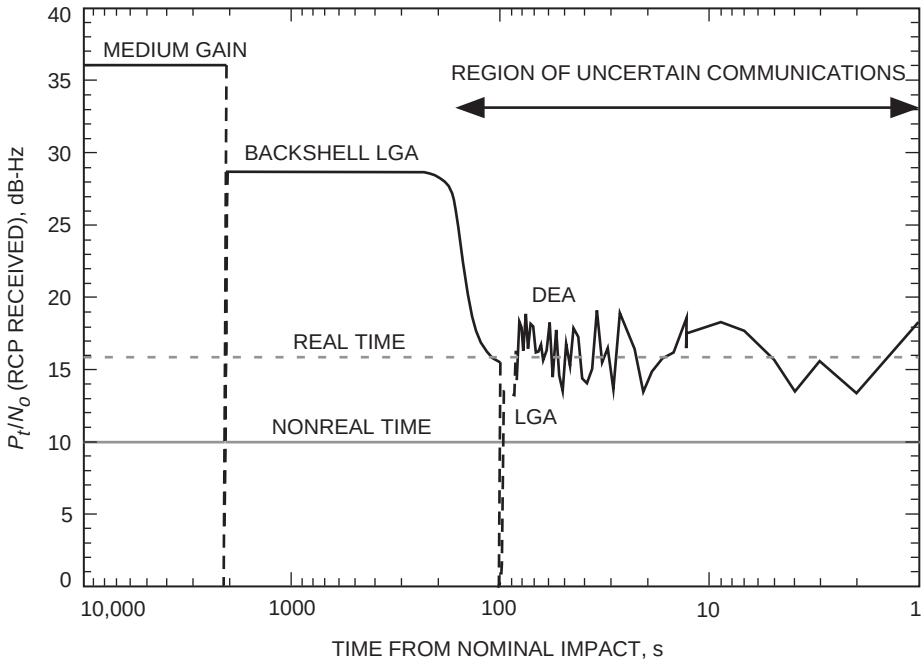

Fig. 2. Expected signal level behavior during EDL.

interval of the frequency shift was a strong function of the arrival flight path angle (FPA), which was not known with sufficient accuracy until just before the beginning of track at DSS 63 for the EDL pass. This required a complex predicts development and selection strategy that is subsequently discussed in this article. The calculated expected Doppler during entry is graphically displayed in Fig. 3, which also illustrates the Doppler sensitivity to FPA.

In the 4 hours after landing, the spacecraft had much work to do. First the airbags were retracted. Then the petals were opened. The airbags were then retracted further. Throughout this work, the lander reported its progress through carrier semaphores. When the EDL sequence was complete, the telecommunications equipment was configured for digital data transmission that would occur once the Sun and Earth were high enough in the Martian sky to assure a reliable link.

III. Spacecraft Telecommunications Configuration

The spacecraft telecommunications equipment supporting the X-band downlink is shown in Fig. 4. Only the downlink paths are shown since all EDL communications were incoherent and performed in the one-way tracking mode. Power values and losses are shown as lumped elements in Fig. 4, whereas in reality they are distributed properties of the hardware. The auxiliary transmitter (AXT) was not used during EDL but is shown for completeness. Similarly, the high-gain antenna (HGA) was not used during EDL.

Of particular note is the "antenna stack" consisting of the MGA, BLGA, and LGA. The MGA is a circular horn antenna affixed to a section of waveguide that fits snugly into the aperture of the BLGA. The BLGA is similarly affixed to a waveguide section that fits into the aperture of the LGA. The LGA is permanently attached to the lander. These three antennas together are much like a telescope with sections that mechanically separated and were shed as the EDL sequence progressed. Only the LGA remained as a final remnant of the "stack" after landing.

The DEA is shown at the far left of Fig. 4. The DEA is a spring-loaded half-wave dipole that automatically deployed when the lander descended out of the backshell. The singular advantage of the

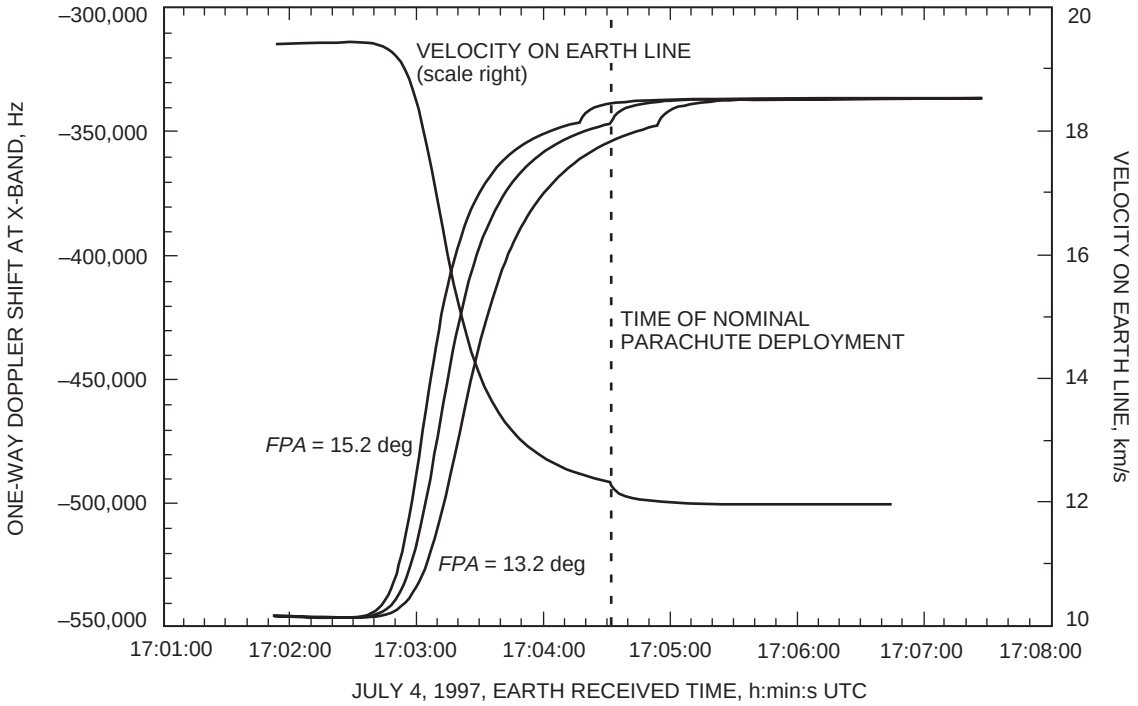

Fig. 3. Expected Doppler shifts during EDL.

DEA is that its peak performance is at a right angle to the terminal descent vector and thus provided coverage at an aspect angle where the stack antennas were poor performers. Otherwise, the DEA, with its linear polarization and lossy coaxial feed line, is unsuitable to support communications at planetary distances.

The spacecraft transmitter operated continuously during EDL and for several minutes after the lander rolled to a stop on the surface of Mars. With roll stop confirmed, the spacecraft transmitter was turned off to conserve battery energy since the landing site was still in darkness. During the next 4 hours, the transmitter was switched on only for brief intervals, constituting semaphores, indicating deployment progress. The timing of these surface semaphores was dependent on landing geometry and subsequent deployment events and could not be predicted with certainty. As a result, recordings continued with the DSP and FSR throughout the entire 4-hour period.

The DEA was used for transmission of all post-landing semaphores except for the final confirmation that the EDL sequence had completed. That semaphore was transmitted via the LGA and was distinguished from other surface semaphores by the presence of only right-hand circularly polarized power in the receivers of the DSN.

IV. Deep Space Network Configuration

Support for EDL communications and lander deployment was solely from Signal Processing Center 60 (SPC 60), with the 70-meter DSS 63 being the prime station. A simplified schematic showing the functional configuration at DSS 63 is presented in Fig. 5. As previously discussed, open-loop recordings were made by both the DSP and the FSR using both RCP and LCP reception. The two Block V receivers were both placed on the RCP branch since the BLGA was in use at the time of entry and the downlink was exclusively RCP. The Block V receivers lost lock, as expected, shortly after entry.

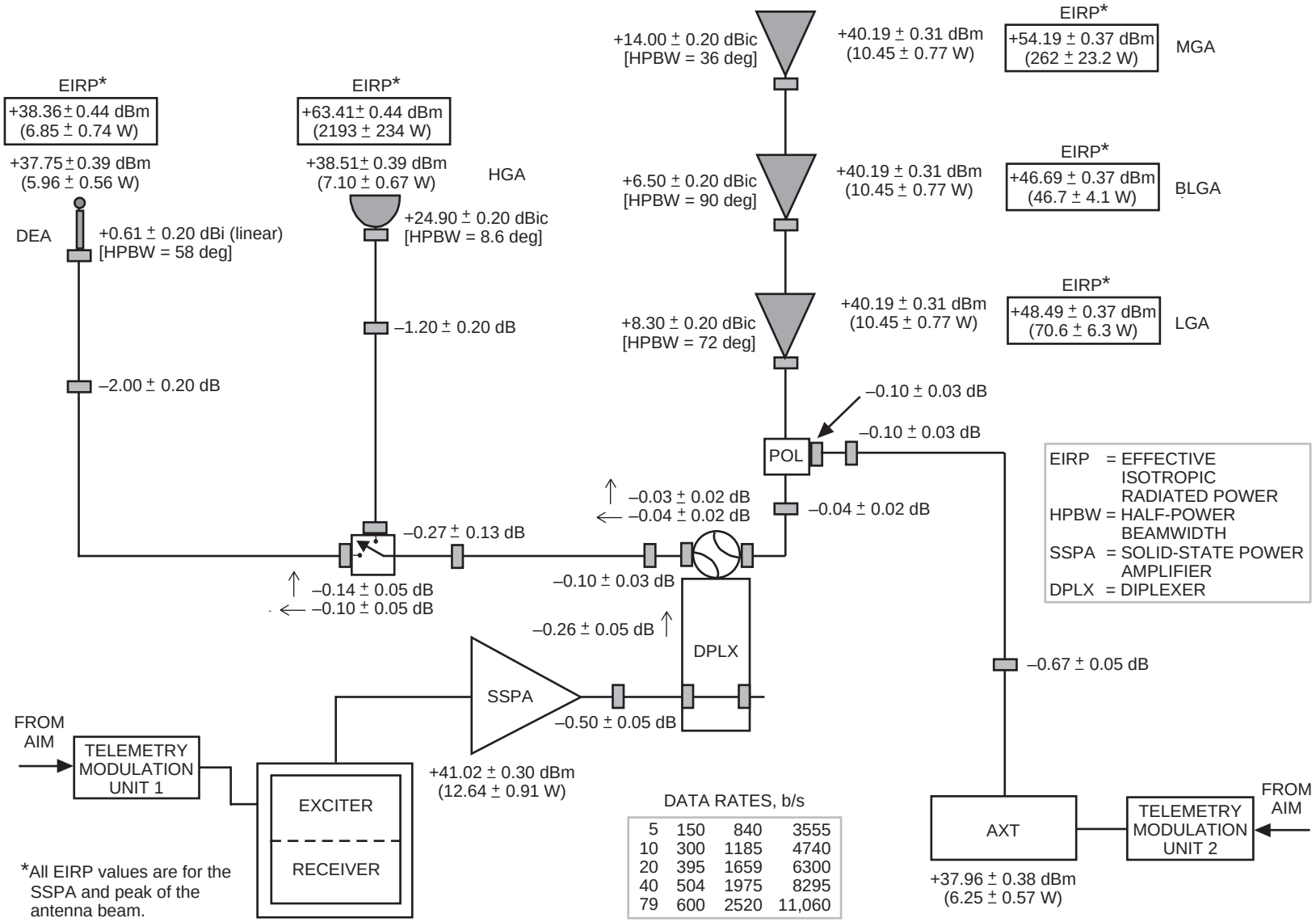

Fig. 4. Mars Pathfinder telecommunications downlink (all tolerances are estimated 1-σ values).

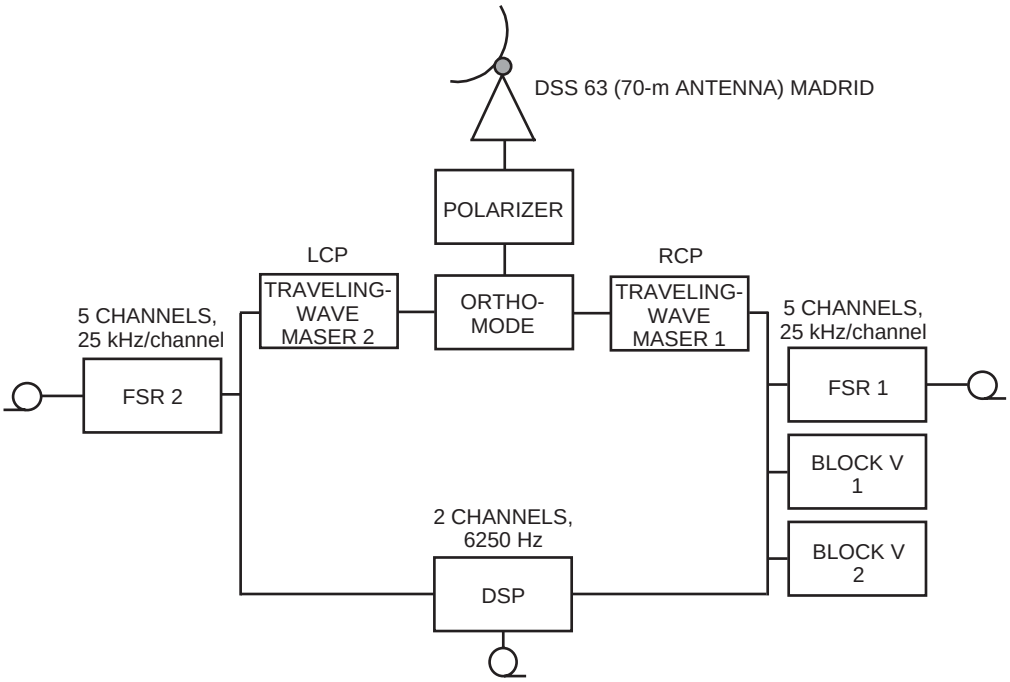

Fig. 5. Ground system configuration at the Madrid Communications Complex.

Originally designed for radio science occultation and relativity experiments, the DSP is the controller and data recorder of the open-loop receivers.[1] The DSP was configured with two channels, each at a 6250-Hz noise bandwidth, to record RCP and LCP during EDL. However, once on the surface of Mars, the DSP receiver filters were reconfigured to a 2-kHz noise bandwidth to enhance sensitivity in the real-time displays.

Originally constructed as part of the Galileo telemetry system [1], the FSR components are shown schematically in Fig. 6 in a simplified manner. The digitizer receives a 300-MHz IF analog input and digitizes it to produce a 256-MHz digital output. A 16-MHz band within this stream is then downconverted to baseband to produce a 16-MHz digital output. The position of the 16-MHz band is able to be set via a configuration table but is fixed for the duration of a pass. Each 16-MHz sample consists of 8-bit in-phase (I) and quadrature-phase (Q) data samples plus timing bits.

With the time tags adjusted to make the output samples effectively delayed to the center of the Earth (a function that was not necessary for this application but was an active part of the instrumentation), the signal is next fed to a set of tone boards consisting of 16 tone rotators. Each rotator selects a narrow bandpass from the 16-MHz signal and converts it to baseband by applying a phase rotation determined by integrating a frequency model every millisecond. The frequency of any detected signal is, thus, the residual between the observed and the predicted frequency. The digitizer/downconverter, delay board, and tone boards are under the control of a single-board VME MC68040 processor, called the real-time processor (RT), which in turn is connected to a Sun workstation data processor (DP) via a point-to-point ethernet. The VME processor reads the results of the tone boards every millisecond and sends a buffer of data to the Sun processor every second, where it is recorded on disk and on 8-mm tape.

During Galileo operations, nine of the tone rotators are used to record the carrier and upper and lower four harmonics of the Galileo signal, with each rotator producing at a maximum rate of 6400 samples

[1] S. Asmar and R. Herrera, editors, *Radio Science Handbook*, vol. 6, JPL D-7938 (internal document), Jet Propulsion Laboratory, Pasadena, California, 1995.

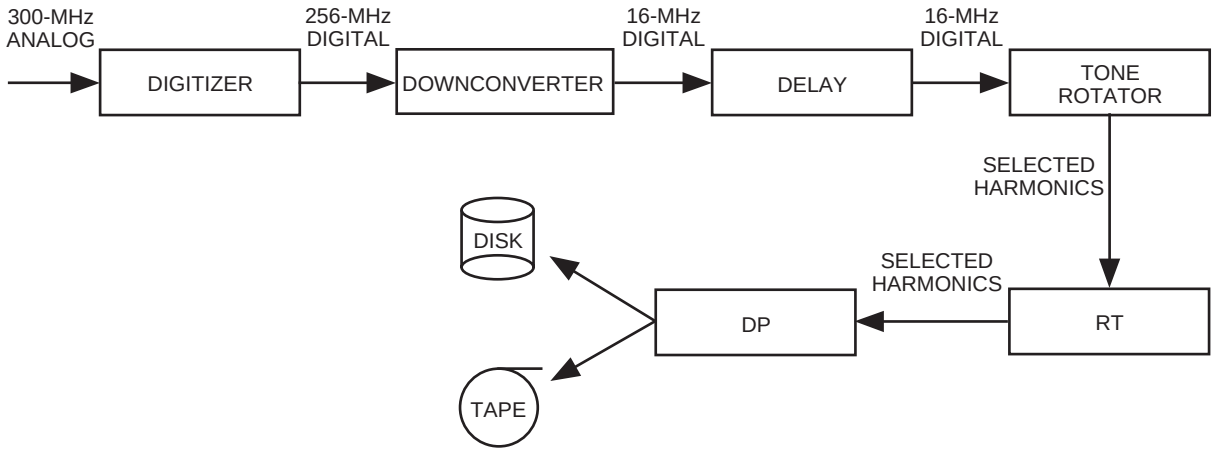

Fig. 6. Data flow in the full spectrum recorder.

per second. For Mars Pathfinder, only five tone rotators were required: one for the carrier, two for the inner harmonics (upper and lower), and two for the outer harmonics (upper and lower). Due to the lower number of harmonics, the sampling rate of each tone rotator could be increased to 25,000 samples per second.

Operating the FSR requires the delivery of delay, frequency, and telemetry predicts. The frequency predicts give the expected frequency of the carrier as a function of time, while the telemetry predicts give the expected subcarrier frequency. The subcarrier frequency is corrected by the predicted Doppler shift, and multiples of the subcarrier frequency are added to the carrier frequency to obtain the phase and phase derivative values that are loaded into the tone board. The predicts were constructed such that the "inner" harmonics were approximately 22.5 kHz on either side of the carrier, while the "outer" harmonics were placed 360 Hz on either side of the carrier. With the given sampling rate, the frequency ranges of the carrier rotator and inner harmonic rotators overlapped. Thus, the three rotators in effect synthesized a single frequency window around the carrier of 70-kHz full width.

Figure 7 shows the dual FSR in its configuration utilized for EDL with an interface between the needed subassemblies. The IF selector switch (ISS) is a 4×4 crossbar switch that allows any FSR to process any one of four IF inputs. Unlike the Galileo application, one FSR was assigned to record the RCP signal while the other was assigned to record the LCP signal. Real-time data were recorded at the station while several of the real-time fast Fourier transform (FFT) displays were transmitted to JPL for monitoring by the project staff.

During Galileo operations where the carrier is suppressed, the FSR searches for the presence of a signal in the upper and lower harmonics. The signal usually is too weak to be detected by simply performing an FFT in these side bands because the data modulation spreads out the signal power over several hundred hertz. In order to make a detectable signal, the FSR multiplies the two side bands together and performs an FFT on the result. The squaring eliminates the data modulation, since every data bit is either $+1$ or -1, which becomes 1 upon squaring. However, this also reduces the signal strength, since the signal-to-noise ratio (SNR) is small to begin with and becomes smaller after squaring. In the original MPF design, the data side bands were expected to be modulated by a 5-Hz data signal. As such, the FSR software used the algorithm described above in its real-time signal detection processing, with the modification that the search was used on both the inner and outer harmonics.

All receivers at SPC 60 were aided by predicts during the events of EDL. Because the FPA remained uncertain until just before entry, it was necessary to build 21 sets of predicts that spanned the control accuracy of the arrival trajectory. Each of the predict sets modeled the approach asymptote, Mars'

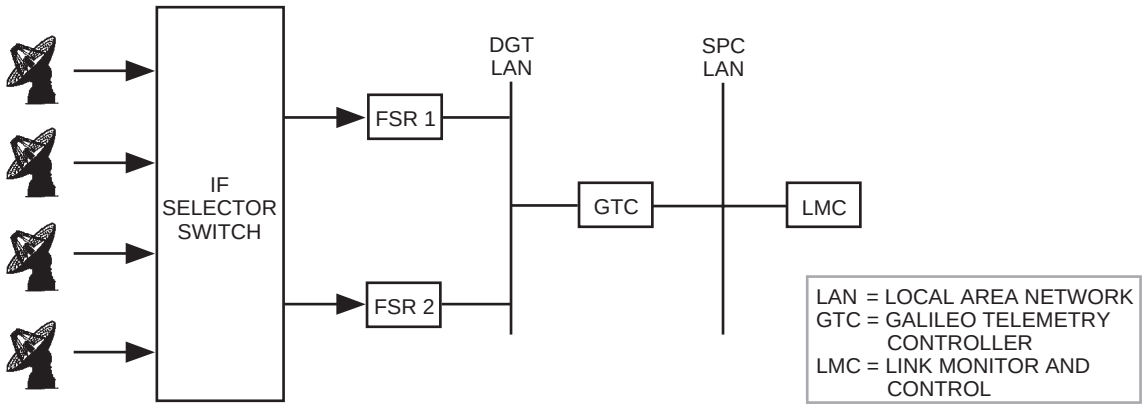

Fig. 7. The FSR dual configuration at the Madrid Complex.

atmospheric density profile, parachute deployment, and Mars' rotation at the coordinates of the landing site. The predict sets were prepared in steps of 0.1 deg for an interval of ±1.0 deg around the nominal FPA of −14.2 deg. The arrival time at Mars also was a sensitive parameter in predicts construction but was so highly correlated with FPA that predicts could be selected using FPA alone.

The knowledge of arrival FPA improved significantly as the spacecraft fell into the gravity well of Mars. FPA updates were procedurally planned beginning at 48 hours before entry. At 24 hours before entry, a predict set called the default set, which was based on the best estimate of FPA at that time, was selected and transmitted to SPC 60. At 1 hour before the DSS 63 beginning of track, a new estimate of FPA was provided by the Pathfinder navigation team. The new value was sufficiently different from that of the default predicts that the decision was made to send updated predicts in accordance with procedures planned much earlier. The update predicts were based on an FPA of −13.9 deg and were the final set used to support EDL.

V. Operations Strategy

The DSP operations did not require any specific hardware or software modifications for this application, although the filter selected for EDL operations had not commonly been used and went through additional testing. The DSP requires only a tuning predict set, as it controls the open-loop receiver's second, tunable, local oscillator (LO). The predict set was updated at the same time as the FSR predict set. It was configured to record the RCP and LCP components of the X-band signal simultaneously. It recorded the data on 8-mm tapes that were copied after the pass for backup.

No hardware changes were needed to support EDL communications at the FSR level. However, in order to record the higher data rates and implement the EDL signal-processing algorithms, a different configuration file as well as a different version of the software needed to be loaded into the FSRs. This version was loaded into a temporary directory and activated via a software switch. The operator had to load the proper configuration table and the specified predict set, verify the system, and run it at a specific time. Care had to be taken not to start the pass too early since, due to the increased sampling rate, there was insufficient disk space to store the data from the entire pass. During the pass, operator activity was minimal except for the occasional entry of a frequency offset command to add a real-time offset to the predicts to keep the signal within the small real-time frequency analysis window (see below). At the end of the pass, the operators made an additional copy of the tapes for backup and sent the originals to JPL for further analysis.

VI. Real-Time Operations

The DSP computed real-time FFTs that were displayed at the station and also transmitted to JPL. In addition, the stability analyzer, a device used for diagnostic measurements of radio science instrumentation, also was used to compute much faster and higher-resolution FFTs for local display at the station. The stability analyzer did not record any data.

The real-time analysis of the FSR was central-processing-unit (CPU) constrained due to the large number of cycles taken up on the FSRs by the data reception and recording. Enough CPU time was available to launch one analysis "cycle" every 15 seconds, with each cycle consisting of a 4-second carrier FFT and a 15-second FFT for the inner and outer side bands using the algorithm described above. The carrier FFT spanned only ±500 Hz around the expected frequency, and the side band analysis was dependent upon carrier detection for proper operation.

VII. Real-Time Analysis

Figure 8 shows, in Earth-received times (ERTs), the residual RCP and LCP carriers over several hours encompassing the end of cruise phase, atmospheric entry, landing, and deployment of the low-gain lander antenna. Gaps in the data indicate times that no statistically significant peak was detected in the FFT. The spacecraft cooling system was vented at approximately 15:30, and the first section of the plot shows the resulting rise in the residual frequency due to the thermal dependence of the onboard oscillator. There are no breaks in the data during this time except for a loss of signal from approximately 16:32:30 to 16:33:00, corresponding to cruise-stage separation. As expected, no LCP signal was detected during this time.

The period of time shortly after 17:00 is shown in more detail in Fig. 9. The arrows in the plot indicate the predicted times of selected spacecraft events. The RCP signal was lost shortly before peak deceleration. At 17:05:03, the spacecraft was expected to switch to the EDL antenna so that further transmissions should have been detected in both the RCP and LCP channels. As expected, when the signal returned at 17:10:48, it was detected in both polarizations. Shortly after the signal was detected, the spacecraft turned off its transmitter to conserve power, although this appears to have happened later than predicted.

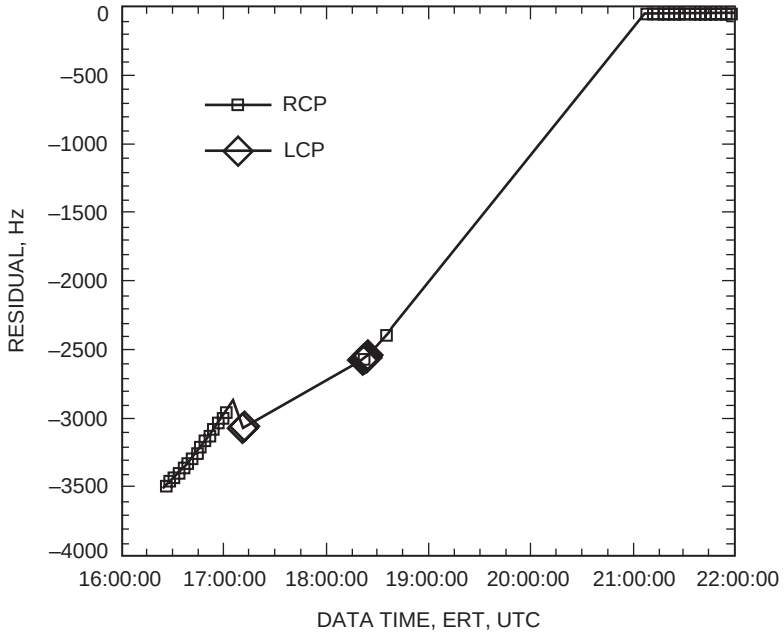

Fig. 8. Real-time carrier residual in the FSR.

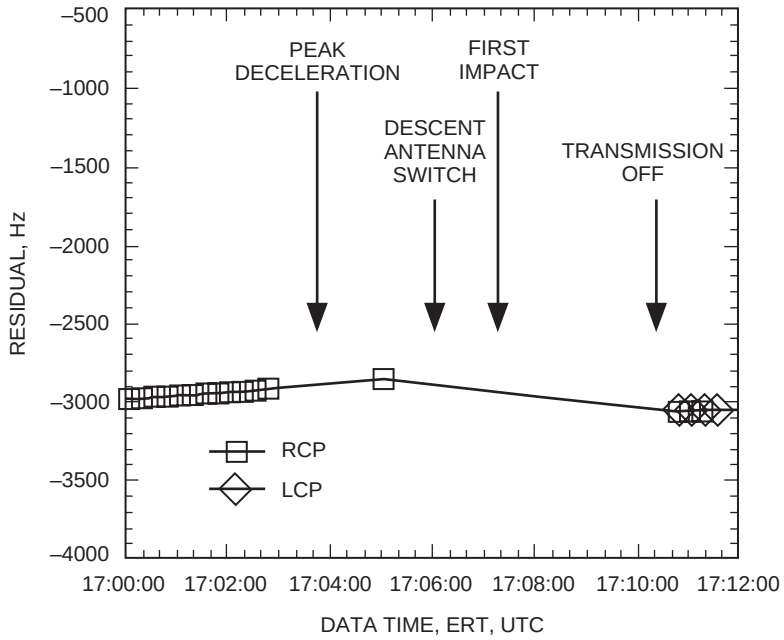

Fig. 9. A close-up of real-time carrier residual in the FSR.

Figure 10 shows a more detailed view of the period between 18:10:00 and 18:45:00. The spacecraft was expected to make another transmission on the EDL antenna after the air bags had been retracted, and in fact such a signal was detected at 18:22. Note that the signal was detected several minutes later than expected. One more transmission was anticipated after the lander had opened its petals and switched to the lander low-gain antenna. The expected signal arrived at 18:34 and was detected only in the RCP channel, consistent with the polarization of the lander low-gain antenna. The lander again shut off its transmitter to conserve power and did not turn it on again until the three-way session began at 21:07. This corresponds to the portion of Fig. 8 in which the residual frequency is close to zero.

No side-band semaphores were detected in the real-time analysis.

VIII. Post-Pass Analysis: EDL Carrier Detection

Pathfinder's descent sequence presented a unique challenge to recovering its carrier frequency on Earth. Not only were large Doppler frequency shifts imposed during braking, but after parachute deployment, the signal amplitude fluctuated considerably as the spacecraft spun and swung at the end of its tether.

Of primary interest was peak deceleration, when the spacecraft slowed from 7 km/s to approximately 0.3 km/s. Reconstruction of the Doppler profile for this period would enable science investigators to pin down the pressure–temperature profile of the upper Martian atmosphere, as well as a number of other parameters concerning the spacecraft trajectory. Unfortunately, due to extreme sensitivity to modeling error, the receiver tuning predicts proved inadequate for maintaining a trackable carrier in band. Figure 11, which duplicates the sensitivity of the real-time display, shows a 2-minute gap in power and frequency versus time for the recorded DSP data. The signal, moving at such a rate that its energy smeared across too many FFT bins, simply disappeared from view, only to reappear when the Doppler returned to nominal in the brief moment before parachute deployment.

After parachute deployment and until the spacecraft came to a complete stop, the signal faded in and out as the antenna rotated toward and away from Earth. Frequency data from this period, also shown in Fig. 11, would help confirm accelerometer data concerning the number and duration of bounces.

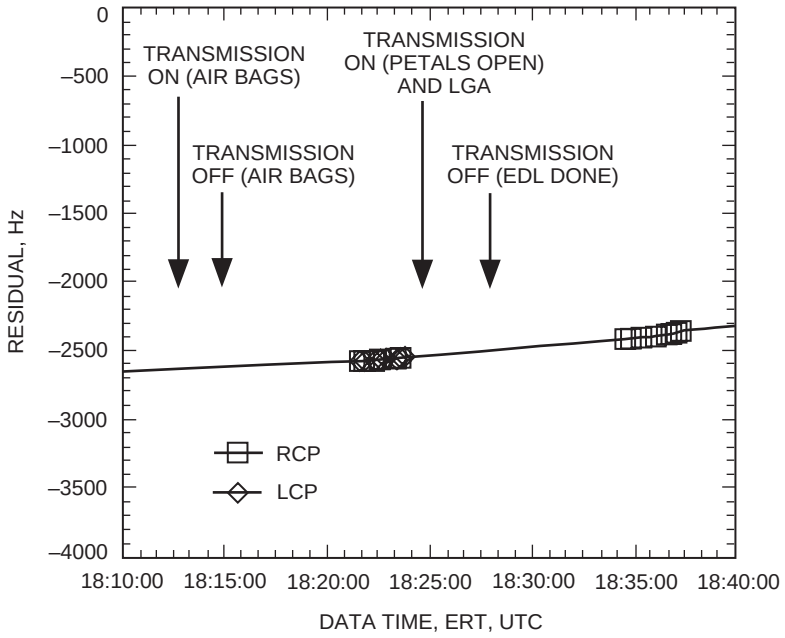

Fig. 10. A close-up of real-time carrier residual in the FSR in another time region.

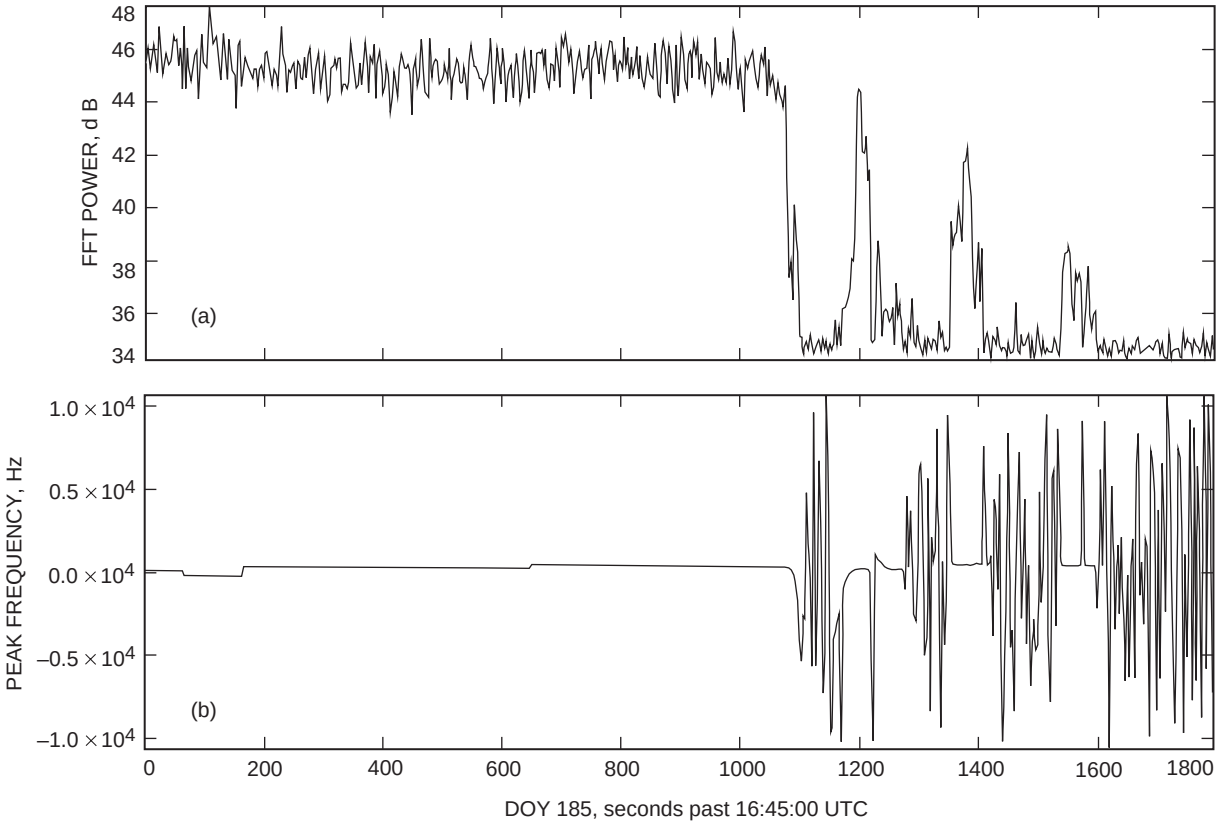

Fig. 11. The static FFT detection results for the EDL time period from 16:45:00 to 17:15:00 UTC: (a) power and (b) frequency.

The strategy used to obtain precision Doppler estimates started with coarse estimates from a ramped FFT search later used to guide steered-phase-locked-loop detection. A ramped FFT search involves pretuning the signal, at each instant, with a range of frequency ramp rates and choosing the one that produces the strongest FFT signal power (i.e., the least amount of smearing). For signals with high Doppler dynamics, ramped FFTs offer the possibility of filling in the gaps of a static FFT detection. Ramped FFTs have a coarse frequency resolution, and a model local oscillator constructed from the ramped estimates was steered from the original signal, allowing a phase-locked loop (PLL) with a 3-Hz loop bandwidth to track the residual. Figure 12 shows the detection strategy in block diagram form.

Figure 13 shows a waterfall plot from the ramped FFT search, depicting peak power versus ramp rate as a series of lines stacked vertically to represent increasing time. The plot shows about 100 seconds around the peak deceleration event. The line of peak ramp rates effectively represents the derivative of the recorded carrier. During processing, the ramp search range gradually was widened as the full extent of predict error was realized. In fact, it soon was realized that the carrier quickly moved beyond the 6-kHz DSP bandwidth; current and subsequent plots come from the much wider (25-kHz) FSR data set. However, even with a search range covering −2000 Hz/s to 1000 Hz/sec, there remained a period of 30 seconds during which no signal was detected. Once the peak ramp rate of a given instant of time has been detected, the peak baseband frequency, Fpk, can easily be derived by

$$Fpk = Fpk_{fft} + Rpk\frac{\tau}{2} \tag{1}$$

where Fpk_{fft} is the peak FFT bin after deramping, Rpk is the peak ramp rate, and τ is the measurement interval, in this case 3 seconds (7500 point FFTs; 10 averages). Figure 14 plots the peak frequency versus

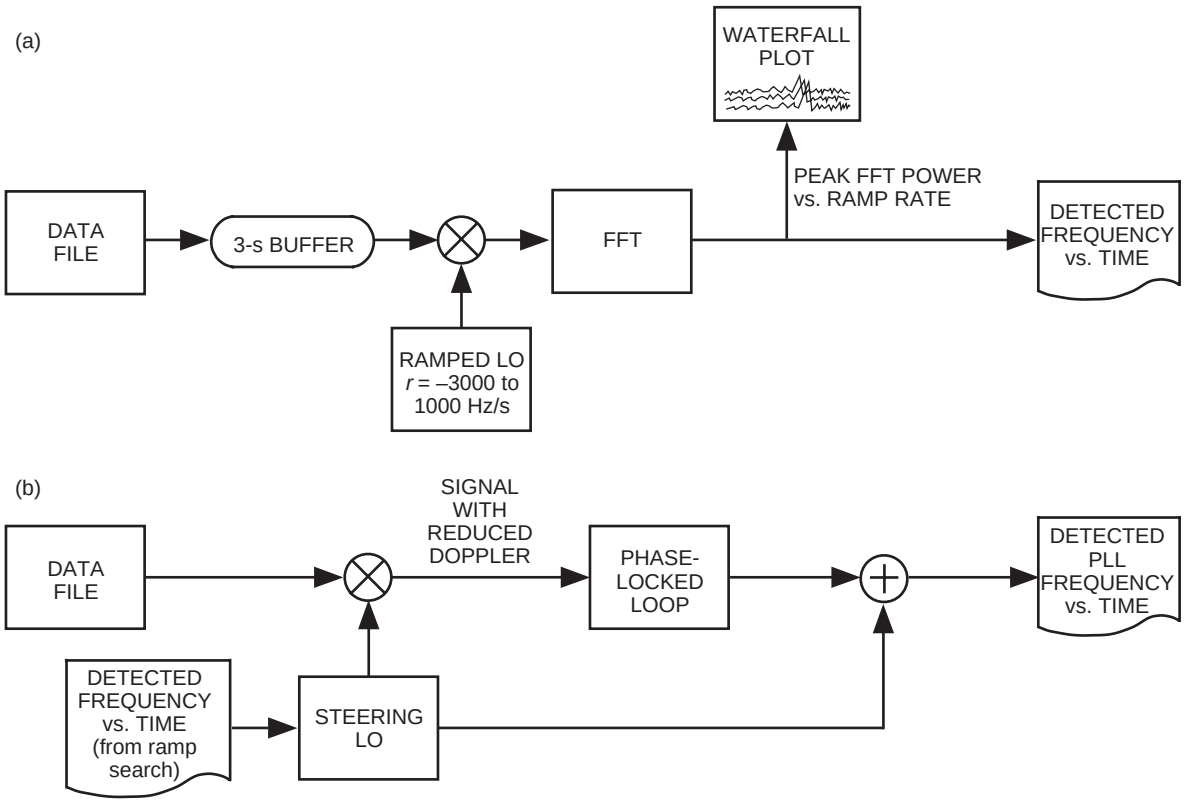

Fig. 12. The detection strategy: (a) the ramped-FFT detection architecture and (b) PLL detection of residual frequency.

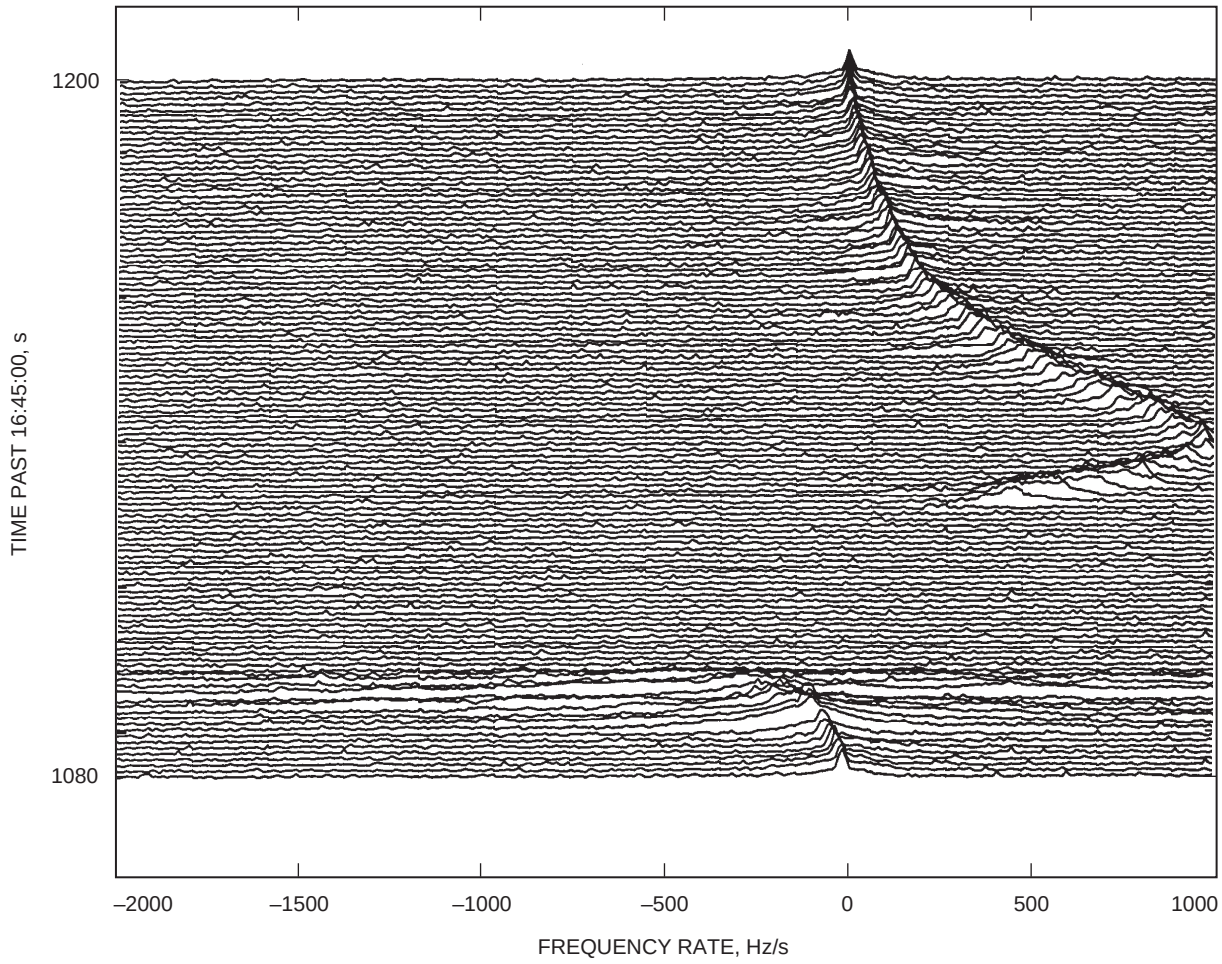

Fig. 13. A waterfall plot showing the peak ramp rate (i.e., signal derivative) versus time for the peak deceleration event. Note the 30-s signal outage beginning at about 17:03:20 UTC (1100 s past 16:45:00).

the time of the interval shown in Fig. 13. Note that when the signal returns after the 30-second gap, the predict error is so great that the carrier has been replaced by a 22.5-kHz subcarrier side band that has shifted into the carrier channel. A few seconds later, the carrier appears at the other side of the band heading for 0 Hz, just as the subcarrier crosses back into the subcarrier channel.

There are several possible explanations for a 30-second signal outage at peak deceleration:

(1) Excessive vibration from braking destroyed the coherency of the auxiliary oscillator, either through high-frequency random Doppler shifts or by disturbing the oscillator itself.

(2) Ions from the ablating heat shield formed a plasma cloud behind the lander, blocking transmission to Earth.

(3) Ions from the same process funneled into the antenna waveguide, causing some sort of ion breakdown or coronal discharge.

(4) Actual chunks from the disintegrating heat shield collected in the vortex behind the lander, blocking the signal path to Earth until either the descent angle changed or the pieces broke away. Whatever the process involved, it wouldn't have to be a very large effect to reduce the roughly 12-dB SNR signal below the detection floor. Efforts to use the subcarrier channels as a more sensitive detector are discussed below.

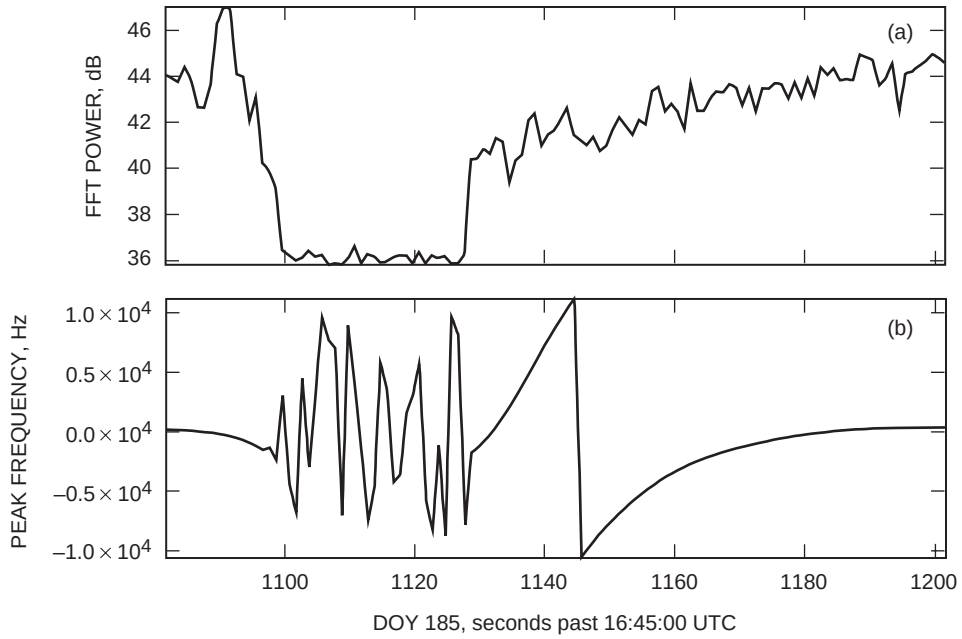

Fig. 14. The ramped FFT detection results at peak deceleration, showing subcarrier in band at 1130 s, followed by carrier at 1147s: (a) FFT power and (b) peak frequency.

Figure 15 shows the final data set of detected sky frequencies and signal power for EDL (minus the subcarrier-detected data at peak deceleration). Detected sky frequency, or received X-band frequency at antenna input, is formed by subtracting the detected baseband frequencies from the FSR-predicted sky frequencies. The final data set contains both PLL and ramped FFT data, which can be distinguished in the power plot by the jump in level between the two detection methods (PLL data near 13 dB and FFT data near 40 dB), since both use differently referenced dB power units. The three early power dropouts in the PLL data are from a set of frequency offsets applied to center the carrier in the FSR bandwidth.

Figures 16 through 18 present a closer view of the detected sky frequencies (and predicted sky frequencies) for peak deceleration, parachute deployment, and the impact period, including several bounces and rolls upon the Martian surface. Figure 16 shows deceleration beginning about 7 seconds early, while Fig. 17 shows the parachute deployment beginning about 5 seconds late (about 7:05:21 ERT) compared with the predicts. About 50 seconds after parachute deployment (Fig. 18), the signal drops below threshold, but still fades in and out every few seconds until a strong surge in signal strength occurs at about the time of rocket ignition (17:07:30). This strong signal continues for about a minute as impact and several bounces occur, with sudden jerks in oscillator frequency (50 to 300 Hz), either from Doppler shift or the electronics being jarred. The signal disappears again for about 2 minutes and then returns one last time (17:10:40 ERT) for about a minute as what looks like a few final rolls are detected.

IX. Additional FSR Data Analysis

Detailed analysis of the FSR tapes was performed on the EDL data. The carrier FFT range was increased from ±500 Hz to ±12,000 Hz and the integration time reduced to 1 second. In addition, frequency rates between −2000 Hz/s and +2000 Hz/s in steps of 20 Hz/s were applied to the data before the FFTs were taken, and only the FFT with the largest power was taken for any given second. Figure 19 shows the results of this analysis. The signal is still lost near the peak deceleration, though the time period of the outage (from 17:03:18 to 17:03:47) is much shorter than the off-line analysis. The feature from 17:03:48 to 17:04:05 presumably is due to a deviation from the predicts larger than 12.5 kHz so that

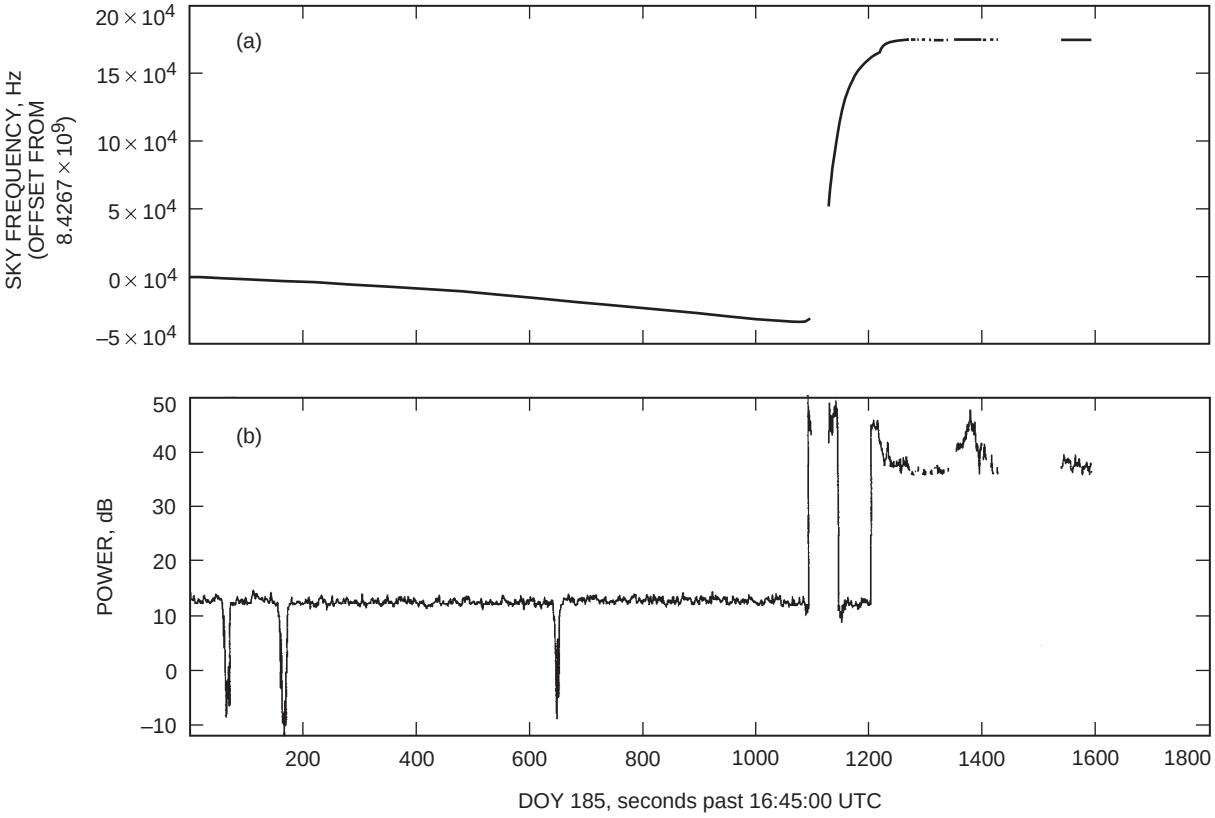

Fig. 15. Detected EDL (a) sky frequency and (b) power versus time, combing both ramped FFT results and PLL fine tuning.

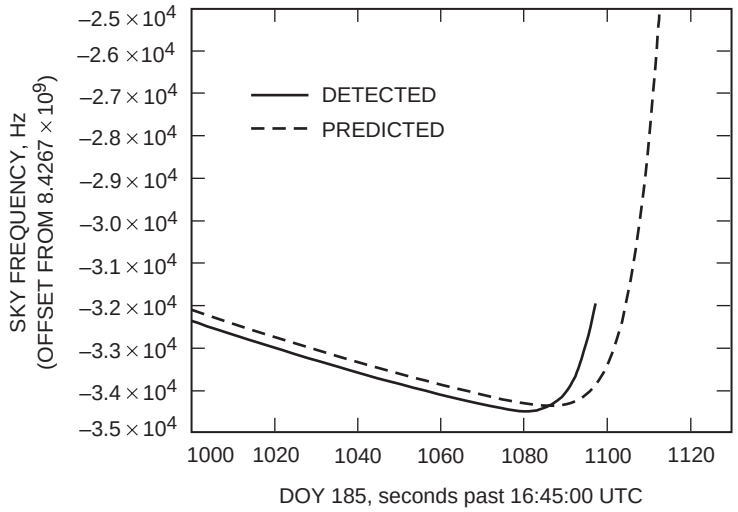

Fig. 16. A closer view of the signal before peak deceleration, showing detected and predicted sky frequencies.

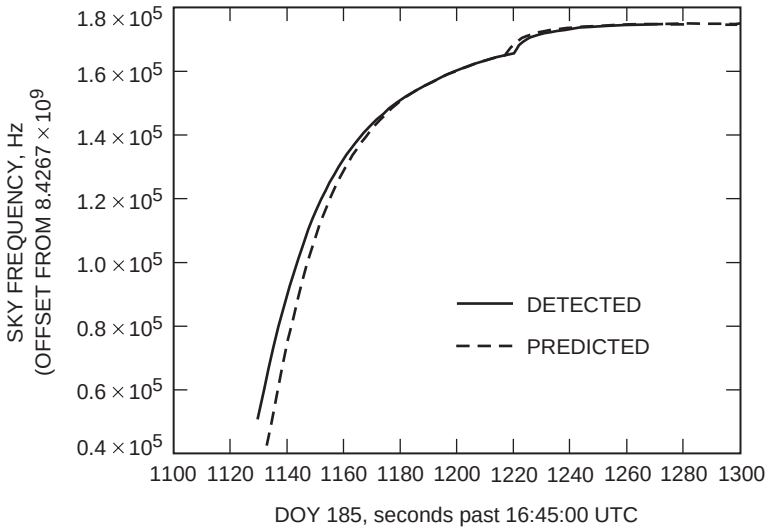

Fig. 17. A closer view of the signal after return from peak deceleration, including parachute deployment at 1221 s (17:05:21 UTC).

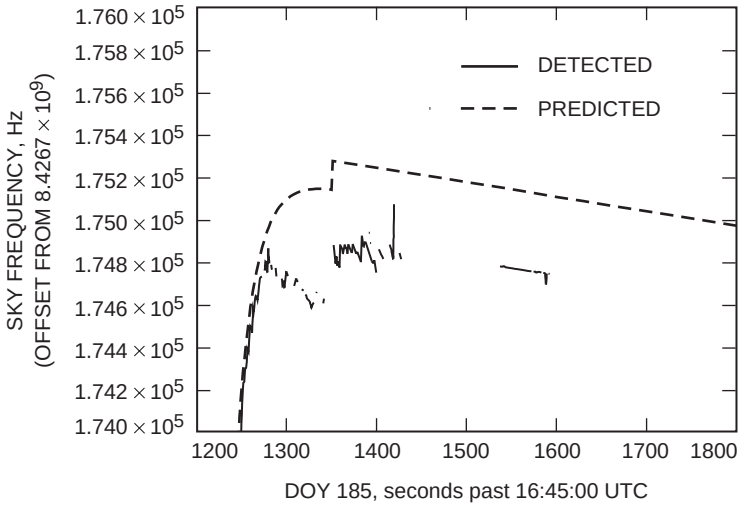

Fig. 18. A closer view of the signal after parachute deployment, showing gradual fade out followed by a strong signal near impact at 1350 s (17:07:30 UTC) and a second fade out followed by a final detection at 1540 s (17:10:40).

the signal from one of the inner side bands was recorded in the carrier channel. The signal passed quickly through the carrier channel and was replaced by the actual carrier. The dip at 17:05:22 presumably is due to the parachute deployment. The LCP signal is seen at 17:06:44 and 17:07:09, shortly after the expected switch to the EDL antenna, but no RCP signal is seen during this time. When the RCP signal is clearly detected for several seconds from 17:07:23 to 17:08:40, no LCP signal is detected during the same interval. Finally, from 17:10:39 to 17:11:42, both LCP and RCP carriers are seen clearly.

The off-line detection of the side-band semaphores used a different algorithm from that used in the real-time analysis. Also, during the off-line analysis, it became clear that the predicted subcarrier frequency was inaccurate by approximately 0.3 Hz. (In the outer harmonic, the effect was 16 times larger, or 4.6 Hz.) Thus, an off-line frequency correction was applied to line up the upper and lower harmonics

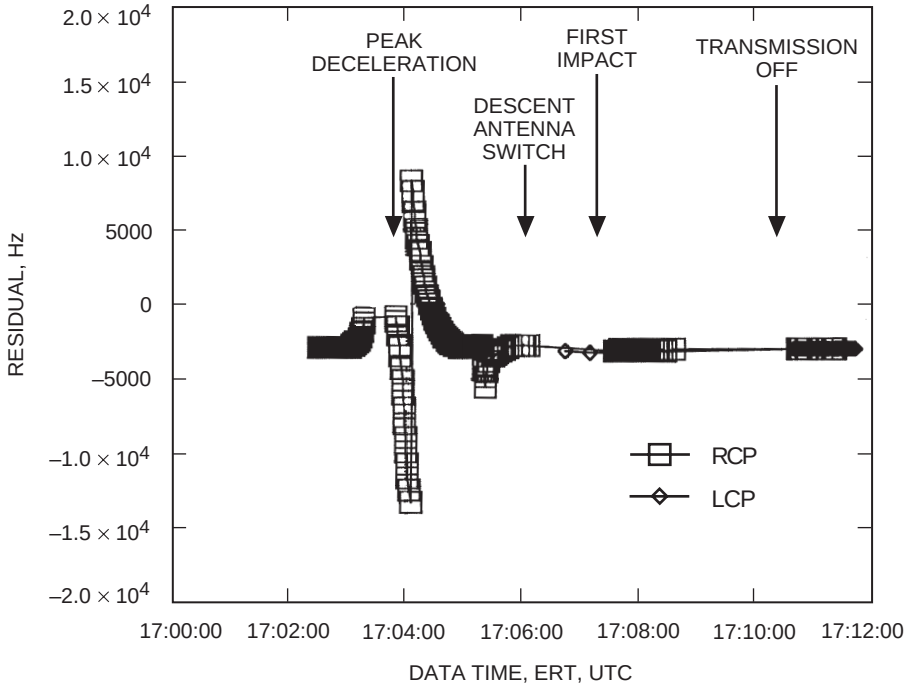

Fig. 19. Additional FSR post-pass analysis.

in frequency, an FFT was performed on each, and the results were incoherently added together. This procedure was applied to both the inner and outer side bands. Even though this procedure removed the residual subcarrier frequency, each harmonic still contained the residual carrier frequency, so FFTs of the inner and outer side bands should have signals at frequencies consistent with that of the carrier.

Figure 20 shows the residuals of the outer harmonic detection for both RCP and LCP. Any point in this plot is a candidate for a side-band semaphore. Two detections are seen in the RCP channel at 17:07:21 and 17:07:33, both of which are consistent with the residual carrier frequency at this time. These are roughly consistent with the expected 600-meter radar detection semaphore, as shown by the arrows in the diagram. An additional RCP signal is seen in the outer harmonic at 17:10:43, but this is almost certainly not a valid side-band semaphore, since the residual frequency is inconsistent with that of the carrier. A clear side-band semaphore is seen in the LCP data from 17:11:07 to 17:11:20. It is peculiar that a similar signal is not seen in the RCP data during this same interval, since both RCP and LCP carriers were detected during this time.

X. Conclusion

The radio science instrumentation at the DSN (DSP and FSR) succeeded in capturing critical information from the spacecraft during the challenging entry, descent, and landing time period. The semaphore signaling technique was shown to work for both side-band semaphores and carrier semaphores. This result has direct applicability to the beacon-mode detection system, which will use a similar scheme to monitor low-power status signals from spacecraft during cruise. It also was demonstrated that multiple tone rotators on the FSR could be used to synthesize a significantly larger frequency range than an individual rotator. This could be useful in future missions with large predict uncertainties similar to those encountered with Mars Pathfinder.

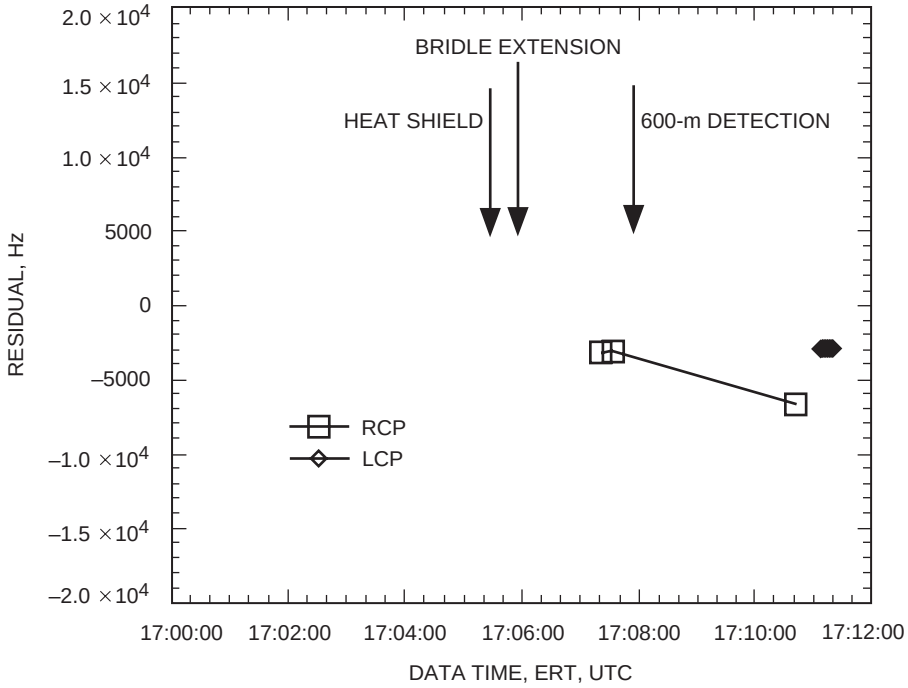

Fig. 20. The outer harmonic residual.

Acknowledgments

The authors thank the management and staff of the Mars Pathfinder Project as well as the management and staff of the Deep Space Network at JPL and the Madrid Complex for their cooperation and hard work in making the EDL communication and signal-recording task successful. Special acknowledgments are deserved by Rob Manning, Greg Kazz, and Anthony Knight. We also thank Sal Abbate and Jeff DeWeese for their support of the DSP and FSR testing and operations as well as Dwayne Chong, Randy Herrera, Aseel Anabtawi, and all the members of the Radio Science Systems Group for the support during all phases of the task.

Reference

[1] T. T. Pham, S. Shambayati, D. E. Hardi, and S. G. Finley, "Tracking the Galileo Spacecraft With the DSCC Telemetry Prototype," *The Telecommunications and Data Acquisition Progress Report 42-119, July–September 1994*, Jet Propulsion Laboratory, Pasadena, California, pp. 221–235, November 15, 1994. http://tda.jpl.nasa.gov/tda/progress_report/42-119/119R.pdf